

Satellite-based retrieval of ice cloud properties using a semianalytical algorithm

A. A. Kokhanovsky

Institute of Remote Sensing, University of Bremen, Bremen, Germany

T. Nauss

Laboratory of Climatology and Remote Sensing, Marburg University, Marburg, Germany

Received 24 December 2004; revised 15 April 2005; accepted 30 June 2005; published 12 October 2005.

[1] A semianalytical algorithm for the retrieval of ice cloud properties from satellite data is presented. The new method is based on the semianalytical cloud retrieval algorithm and uses solutions of the asymptotic radiative transfer theory applicable for optically thick media. Therefore the new method is much less computer time expensive than the commonly used lookup table approaches. Usually, the cloud optical thickness and cloud effective droplet radius are reported for water and ice clouds even though both parameters are dependent on the actual crystal shape assumed in the retrieval procedures. Thus the authors propose to use the reduced optical thickness (ROT) and the particle absorption length (PAL) for the characterization of ice clouds. This implies that no a priori or climatological estimates of the particle shape/size distribution are necessary and increases the comparability of different cloud retrieval algorithms, which are built on many different distribution functions. If still necessary, the retrieved ROT and PAL can easily be transferred to values of the optical thickness and the cloud effective droplet radius by assuming any of those size distribution functions. The developed technique has been applied to data from the NASA EOS Terra Moderate Resolution Imaging Spectroradiometer sensor. The scene shows Hurricane Jeanne just before its landfall near the coast of Florida in September 2004. Both the reduced cloud optical thickness and the particle absorption length have been derived for the eye wall region.

Citation: Kokhanovsky, A. A., and T. Nauss (2005), Satellite-based retrieval of ice cloud properties using a semianalytical algorithm, *J. Geophys. Res.*, 110, D19206, doi:10.1029/2004JD005744.

1. Introduction

[2] Water exists in clouds in liquid, gaseous, and crystalline forms. While remote sensing of water clouds from space is simplified because of the spherical shape of droplets and relative homogeneity of water clouds, crystalline clouds are very inhomogeneous both in vertical and horizontal directions. In addition they consist of ice crystals having very complex shapes [Garrett *et al.*, 2001; Baum *et al.*, 2005a, 2005b]. This complicates retrievals of cloud parameters such as the size of crystals and the optical thickness τ of a cloud. Therefore effects of inhomogeneity are ignored in operational ice cloud retrievals and ice crystals are defined in terms of some a priori assumed specific particle size/shape distribution functions [Platnick *et al.*, 2003; Baum *et al.*, 2005a, 2005b]. Hence a general approach used for liquid water cloud retrievals is closely followed with the substitution of the spherical particle model by models of crystalline media (e.g., hexagonal cylinders and plates). This means that the retrieved effective

size parameter of ice crystals depends on the assumed model of crystals used in the retrieval.

[3] The task of this paper is to introduce a new parameter—particle absorption length l —for ice cloud remote sensing applications. This parameter is habit-independent and can be used instead of the loosely defined ice grain size in the ice cloud retrieval procedures.

[4] In order to derive ice cloud properties, the authors adapt the semianalytical cloud retrieval algorithm (SACURA) [Kokhanovsky *et al.*, 2003] which is based on the asymptotic solution of the radiative transfer equations as described by van de Hulst [1980] to the special case of ice cloud remote sensing. The modified SACURA is then applied for the retrieval of cloud properties from Hurricane Jeanne using data from the Moderate Resolution Imaging Spectrometer (MODIS) [King *et al.*, 1992] aboard the Terra and Aqua satellites.

2. Semianalytical Cloud Retrieval Algorithm as Applied to Ice Clouds

2.1. Nonabsorbing Channel

[5] In contrast to the commonly used lookup table (LUT) approaches, Kokhanovsky *et al.* [2003] developed

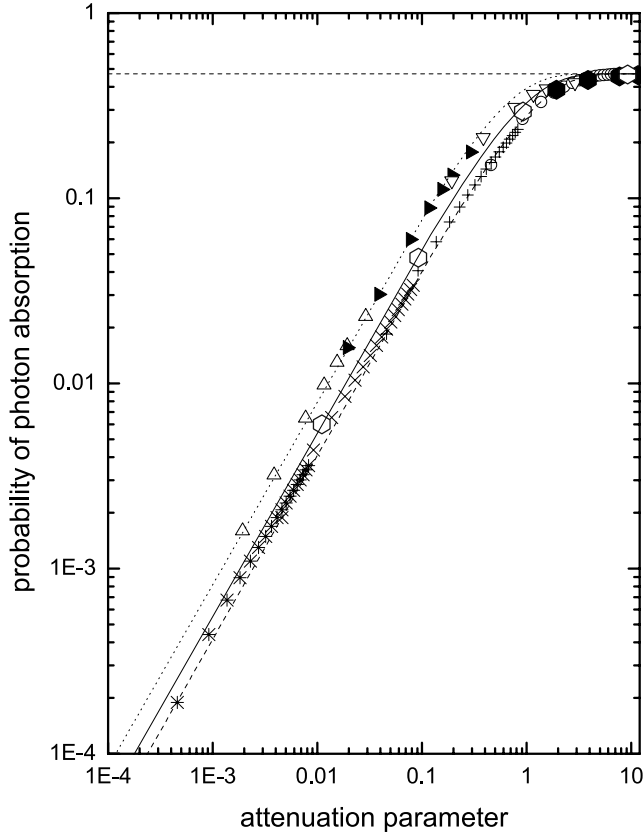


Figure 1. Dependence of the probability of photon absorption β on the attenuation parameter $c = 2a_{ef}/\ell_0$ calculated using the Mie scattering code (circles, crosses, and asterisks, depending on the absorption), the Monte-Carlo geometrical optics code for fractals (triangles, depending on the absorption), and monodispersed randomly oriented hexagonal cylinders (hexagons, depending on the absorption). Lines show the dependence according to equation (16) at $\beta_\infty = 0.47$ and $\ell = BD_{ef}$, where we find that B is equal to 0.9 for spheres (dashed line), 1.2 for hexagonal cylinders (solid line), and 1.8 for fractals (dotted line). The horizontal dashed line corresponds to the asymptotical result $\beta_\infty = 0.47$. Further explanations are given in the text and in Table 1.

a semianalytical cloud retrieval algorithm using the asymptotic solutions [van de Hulst, 1980; King, 1987; Kokhanovsky, 2004a] of the radiative transfer theory. According to van de Hulst [1980] the reflection function

R of an optically thick cloud in a nonabsorbing spectral band can be written as

$$R(\mu, \mu_0, \phi, \tau) = R_\infty^0(\mu, \mu_0, \phi) - t_0(\tau)K_0(\mu)K_0(\mu_0) \quad (1)$$

with the cosine of the solar and observation angle μ_0 and μ , respectively, and the relative azimuth angle ϕ . The diffuse transmittance $t_0(\tau)$ is given by

$$t_0(\tau) = \frac{1}{0.75\tau(1-g) + \alpha}, \quad (2)$$

where g is the asymmetry parameter [van de Hulst, 1980], $\alpha \approx 1.07$, $\tau = \sigma_{ext} L$ is the optical thickness, σ_{ext} is the extinction coefficient, and L is the cloud geometrical thickness. The escape function $K_0(\mu)$ can be described by the following approximate equation for $\mu \geq 0.2$ [Kokhanovsky et al., 2003]:

$$K_0(\mu) = \frac{3}{7}(1 + 2\mu). \quad (3)$$

For a cloud over a reflective ground with Lambertian albedo A_{g0} , the following equation for the cloud reflection function [Kokhanovsky, 2004a] applies instead of equation (1):

$$R(\mu, \mu_0, \phi, \tau) = R_\infty^0(\mu, \mu_0, \phi) - t_0(\tau)K_0(\mu)K_0(\mu_0) + \frac{A_{g0}t_0^2 K_0(\mu)K_0(\mu_0)}{1 - A_{g0}r_0}, \quad (4)$$

where $r_0 = 1 - t_0$ is the spherical albedo for nonabsorbing clouds. Equations (1)–(4) reduce the calculation of the reflection function of a finite cloud to that of a semi-infinite one ($R_\infty^0(\mu, \mu_0, \phi)$), where $R_\infty^0(\mu, \mu_0, \phi)$ depends only on the phase function and even this dependence is rather weak [Kokhanovsky et al., 2003]. $R_\infty^0(\mu, \mu_0, \phi)$ itself can be parameterized [Kokhanovsky, 2004a, 2005] but errors increase with increasing satellite zenith angles and exceed 5% for satellite zenith angles larger than 30° and solar zenith angles larger than 60° [Kokhanovsky, 2004a, 2005]. For nadir measurements the error is below 5% for all solar zenith angles except very low Sun positions close to the horizon which are not suitable for cloud retrievals anyway. While for single case studies and suitable observation geometries the cloud retrieval algorithms perform well with the approximation for $R_\infty^0(\mu, \mu_0, \phi)$ given by Kokhanovsky [2004a, 2005], this approximation is not suitable for operational full-disc applications using geostationary sensors. Then LUTs for the function $R_\infty^0(\mu, \mu_0, \phi)$ must be used [Nauss et al., 2005].

Table 1. Conditions Used in Calculations Presented in Figure 1 Obtained at $n = 1.3^a$

Shape	$A_{ef}, \mu\text{m}$	χ	Method	Reference
Spheres	1–18	1.e-5, 1.e-4, 1.e-3, 1.e-2	Mie theory for polydispersed spheres	Kokhanovsky [2004a]
Fractals	8–119	1.2e-5, 1.2e-4, 1.2e-3, 1.2e-2	geometrical optics	Macke et al. [1996]
Hexagonal cylinders	45	1.2e-5, 1.e-4, 1.e-3, 5.e-2	geometrical optics	Macke et al. [1996]

^aSpherical particles are characterized by the gamma-size distribution with the coefficient of variance equal to 0.38 [Kokhanovsky, 2004a, 2004b]. Fractals are presented by randomly oriented monodispersed Koch fractals of the second generation [Macke et al., 1996]. Hexagonal cylinders are randomly oriented and have the same size (length, 100 μm ; side of the hexagonal cross section, 50 μm). The wavelength used in calculations was equal to 1240 nm for hexagonal particles and fractals. It was set equal to 550 nm for spheres. The value of a_{ef} is defined as $3v/s$, where v is the average volume and s is the average surface of particles in the unit volume of a cloud.

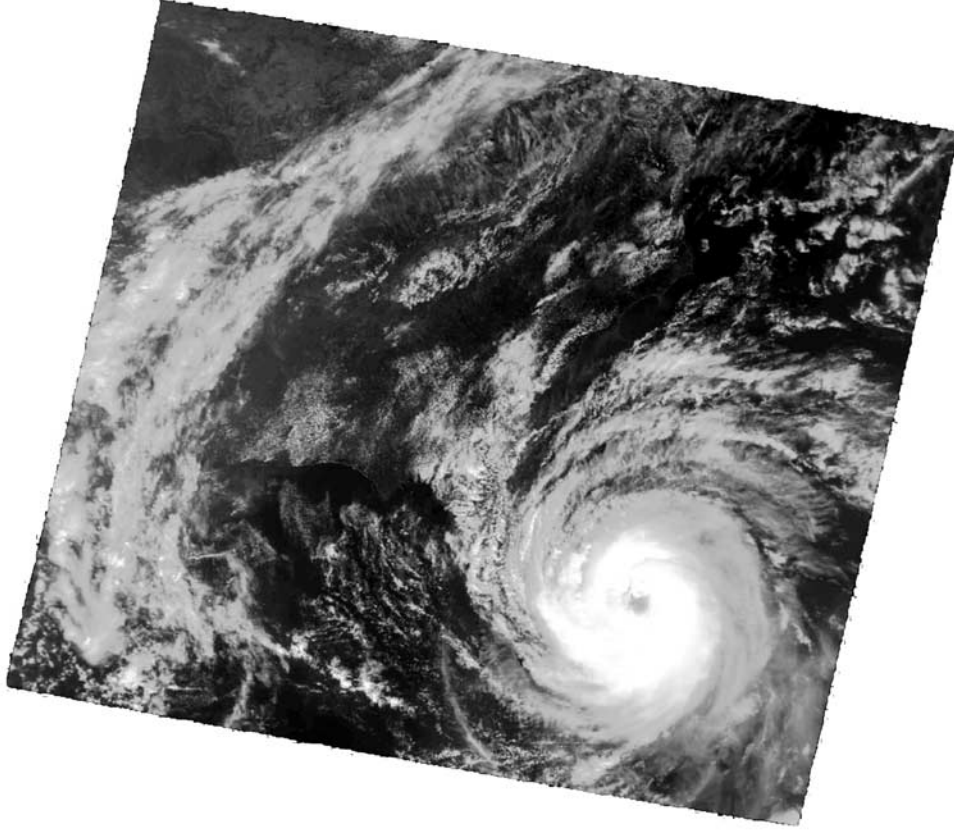


Figure 2. Browse image of Jeanne (25 September 2004, 1615 UTC).

Calculations of $R_{\infty}^0(\mu, \mu_0, \phi)$ require the phase function $p(\theta)$, which can be found using the fractal model of ice crystals as discussed by *Macke et al.* [1996] and confirmed using experimental measurements of crystalline media cloud phase functions [Kokhanovsky, 2003]. In this case, g is approximately equal to 0.74. Very close values of g have been obtained by *Garrett et al.* [2001] from in situ airborne experiments. They found that $g \approx 0.74 \pm 0.03$ for their observations of crystalline media in the visible spectrum. In addition, *Garrett et al.* [2001] underlined that g is almost independent of the particular shape or size of ice crystals in this spectral region. We underline that this value of g can be reproduced using the fractal model of an ice crystal as discussed by *Macke et al.* [1996].

[6] These conclusions allow us to propose the following analytical equation to derive the ice cloud optical thickness τ (see equation (2)):

$$\tau = \frac{4(t_0^{-1} - \alpha)}{3(1 - g)}, \quad (5)$$

where (see equation (4))

$$t_0 = \left[\frac{K_0(\vartheta)K_0(\vartheta_0)}{R_{\infty}^0(\vartheta_0, \vartheta, \varphi) - R(\vartheta_0, \vartheta, \varphi)} - \frac{A_{g_0}}{1 - A_{g_0}} \right]^{-1} \quad (6)$$

or

$$\tau = B_1 \left[\frac{K_0(\vartheta)K_0(\vartheta_0)}{R_{\infty}^0(\vartheta_0, \vartheta, \varphi) - R(\vartheta_0, \vartheta, \varphi)} - \frac{A_{g_0}}{1 - A_{g_0}} \right] - B_2, \quad (7)$$

with $B_1 = 4/[3(1 - g)]$, $B_2 = 4 \alpha/[3(1 - g)]$ leading to $B_1 = 5.128$ and $B_2 = 5.487$ at $g = 0.74$. Similar analytical equations for the cloud optical thickness at nonabsorbing channels have been proposed by *King* [1987], who applied them to water cloud cases, where the value of g depends on the size of particles due to generally smaller radii of droplets as compared to dimensions of crystals. Note that it follows for clouds over black surfaces ($A_{g_0} = 0$) with account for equation (3):

$$\tau = B_1^* \left[\frac{(1 + 2\mu)(1 + 2\mu_0)}{R_{\infty}^0(\vartheta_0, \vartheta, \varphi) - R(\vartheta_0, \vartheta, \varphi)} \right] - B_2, \quad (8)$$

where $B_1^* \approx 0.94$. Equation (8) allows us to obtain the ice cloud optical thickness analytically. The results of the retrieval using this equation are almost insensitive to the size or the shape of ice crystals.

[7] For the case of fractal particles, $R_{\infty}^0(\vartheta_0, \vartheta, \varphi)$ becomes approximately [Kokhanovsky, 2005]

$$R_{\infty}^0(\mu, \mu_0, \varphi) = \frac{A + B(\mu + \mu_0) + C\mu\mu_0 + p(\theta)}{4(\mu + \mu_0)}, \quad (9)$$

where $A = 1.247$, $B = 1.186$, $C = 5.157$ and $p(\theta) = 11.1 \exp(-0.087\theta) + 1.1 \exp(-0.014\theta)$. Here θ is the scattering angle in degrees found from the following equation: $\theta = \cos^{-1}(-\mu\mu_0 + s s_0 \cos \phi)$, where $s = \sqrt{1 - \mu^2}$, $s_0 = \sqrt{1 - \mu_0^2}$.

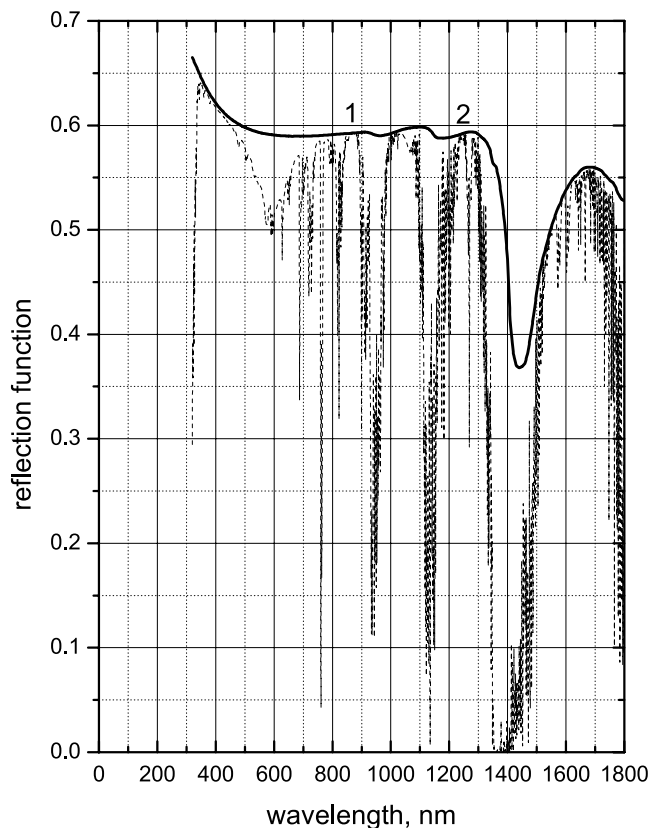


Figure 3. Spectral top of atmosphere reflectance as calculated using SCIATRAN [Rozanov *et al.*, 2005] for two modes: without gaseous absorption (thick line) and with gaseous absorption (dashed line). It was assumed that the cloud has the optical thickness 20 and is illuminated by the solar light at the zenith angle equal to 60° . The satellites observe the scene at nadir. We also accounted for the Rayleigh and aerosol scattering for the model atmosphere as described by Kokhanovsky and Rozanov [2004]. Calculations are performed for water droplets having the gamma particle-size distribution with the mode radius $4\ \mu\text{m}$ and coefficient of variance 38%.

[8] Some research groups report measured values of g for ice clouds as high as 0.82 [Sassen and Liou, 1979] in the visible range (e.g., for clouds composed of solely hexagonal plates). This means that the derived value of τ is biased because of the assumption that $g = 0.74$. This may not hold for all ice clouds, especially for mixed-phase and multilayered clouds, so we advice to report also the retrieved value of the reduced optical thickness (ROT) $\delta = (1 - g)\tau$. The reduced optical thickness is less biased than the optical thickness τ . This is due to the fact that t_0 as obtained from equation (6) is only weakly influenced by the shape of particles because functions $R_\infty^0(\vartheta_0, \vartheta, \varphi)$ and $K_0(\mu)$ change only slightly for crystals of various forms [Kokhanovsky and von Hoyningen-Huene, 2004]. So the reduced optical thickness δ should be mainly reported in outputs of the retrieval algorithms for ice cloud scenes. The optical thickness then can be easily estimated using the relationship: $\tau = \delta/(1 - g)$ and assumed values of g (e.g., $g \approx 0.74$, as discussed by Gerber *et al.* [2000] and

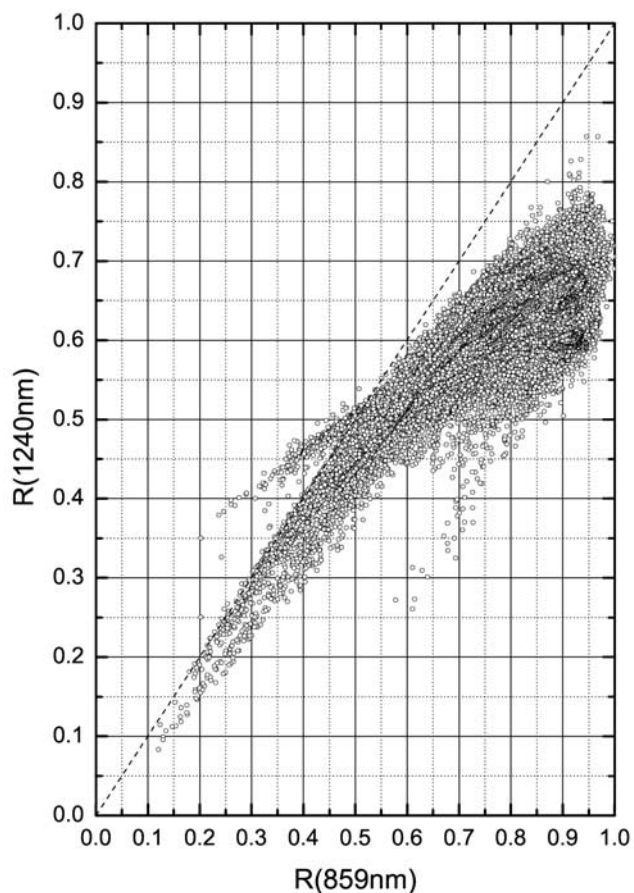


Figure 4. Dependence of the reflection function at $\lambda = 1240\ \text{nm}$ on that at $\lambda = 859\ \text{nm}$.

Garrett *et al.* [2001]. In particular, it follows for ice clouds with fractal crystals: $\tau \approx 4\delta$.

2.2. Absorbing Channel

[9] The case of an absorbing channel (e.g., at the wavelength $\lambda = 1.6\ \mu\text{m}$) is much more complicated.

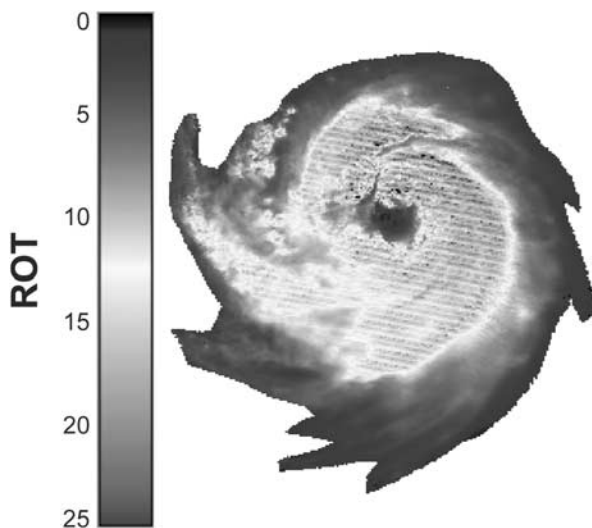


Figure 5. Reduced optical thickness map. See color version of this figure at back of this issue.

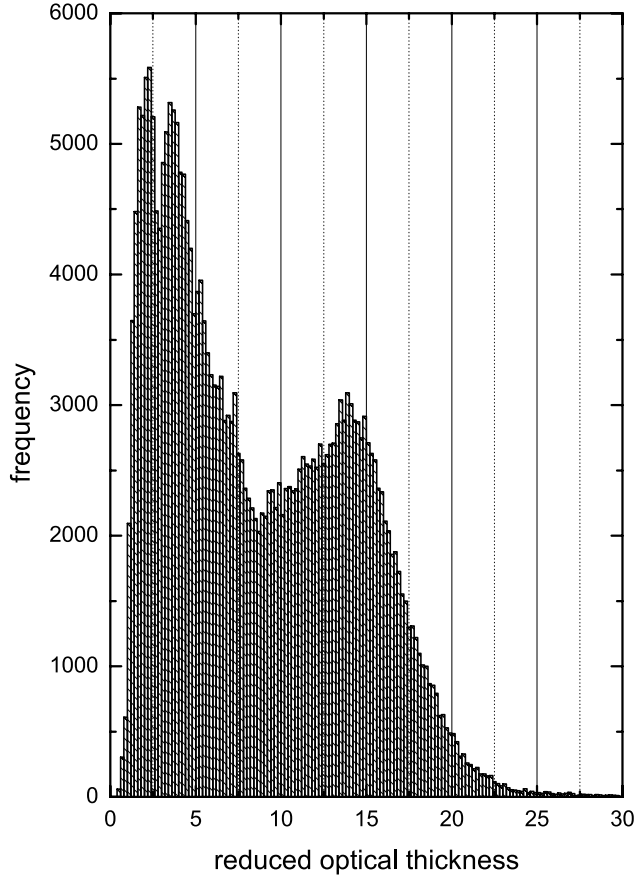


Figure 6. Statistical distribution of retrieved values of the cloud reduced optical thickness.

Instead of equation (4) R for a plane-parallel homogeneous cloud layer overlying the surface with the Lambertian albedo A_g as $\tau \rightarrow \infty$ [van de Hulst, 1980] becomes

$$R(\mu, \mu_0, \phi, \tau) = R_\infty(\mu, \mu_0, \phi) - \frac{mle^{-2\gamma\tau}}{1 - l^2e^{-2\gamma\tau}}K(\mu)K(\mu_0) + \frac{A_g t_d(\mu)t_d(\mu_0)}{1 - A_g r} \quad (10)$$

with the reflection function of a semi-infinite absorbing cloud $R_\infty(\mu, \mu_0, \phi)$ and the escape function of absorbing media $K(\mu)$. Equation (10) is valid for arbitrary values of the single scattering albedo ω_0 . The parameters m , l , γ , and the escape function $K(\mu)$ can be found from the solution of integral equations [Nakajima and King, 1992] and t_d and r give the cloud diffuse transmittance and the spherical albedo for a cloud over a black surface, respectively. Kokhanovsky *et al.* [2003] have shown that equation (10) takes the following simpler form for weakly absorbing channels free of gaseous absorption:

$$R(\mu, \mu_0, \phi) = R_\infty(\mu, \mu_0, \phi) - te^{-x-y}K_0(\mu)K_0(\mu_0) + \frac{A_g t^2 K_0(\mu)K_0(\mu_0)}{1 - A_g r}, \quad (11)$$

where

$$R_\infty(\mu, \mu_0, \phi) = R_\infty^0(\mu, \mu_0, \phi) \exp \left\{ -y \frac{K_0(\mu)K_0(\mu_0)}{R_\infty^0(\mu, \mu_0, \phi)} \right\} \quad (12)$$

$$t = \frac{\sinh y}{\sinh(\alpha y + x)}, \quad r = (1 - te^{-x})e^{-y}, \quad (13)$$

and

$$x = \gamma\tau \equiv 0.75\delta y, \quad y = 4\sqrt{\frac{1 - \omega_0}{3(1 - g)}}, \quad \gamma = \sqrt{3(1 - \omega_0)(1 - g)}. \quad (14)$$

Therefore equation (11) can be written as

$$R(\mu, \mu_0, \phi) = R_\infty^0(\mu, \mu_0, \phi) \exp \left\{ -y \frac{K_0(\mu)K_0(\mu_0)}{R_\infty^0(\mu, \mu_0, \phi)} \right\} - \left(e^{-x-y} - \frac{A_g t}{1 - A_g r} \right) t K_0(\mu)K_0(\mu_0). \quad (15)$$

The accuracy of this formula is studied in Appendix A [see also Kokhanovsky *et al.*, 2003; Kokhanovsky and Rozanov, 2004; Kokhanovsky, 2004a]. It is of a great advantage that equation (15) involves the same functions as those

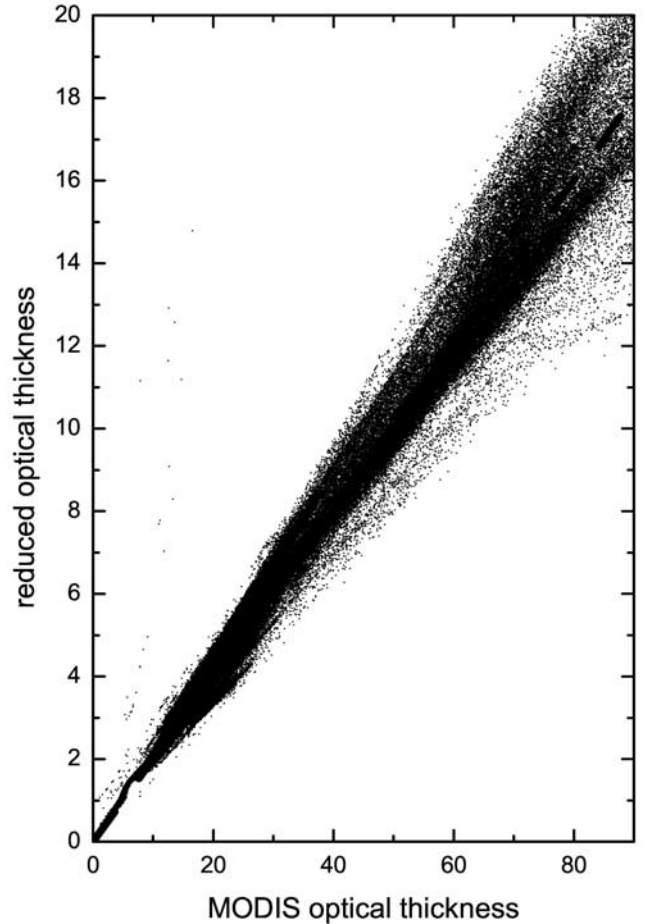


Figure 7. Correlation between values of δ and τ_m .

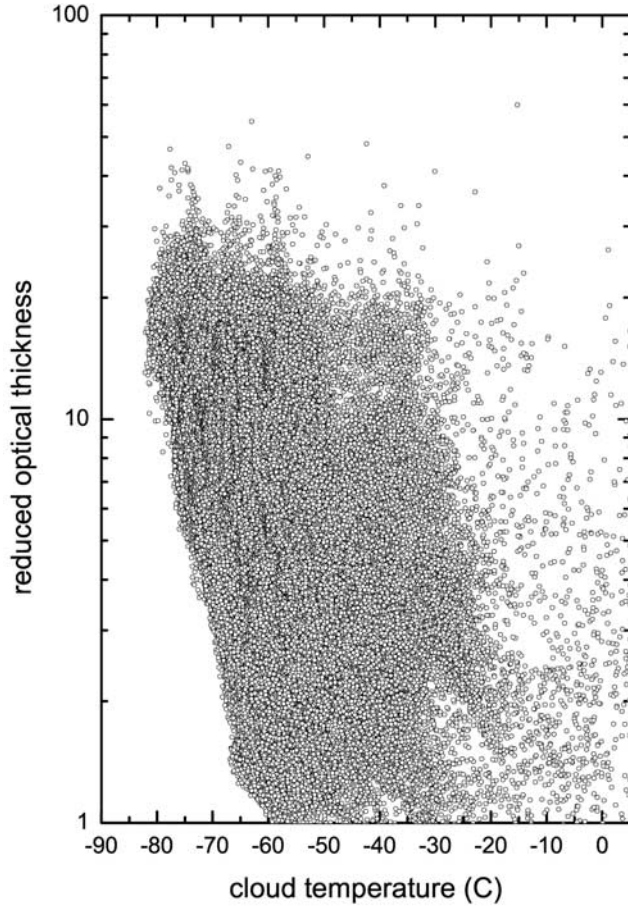


Figure 8. Correlation between the reduced optical thickness and cloud temperature. The cloud temperature was derived using the MODIS cloud retrieval algorithm.

introduced for the nonabsorbing case. If a weakly absorbing wavelength is selected in a close vicinity to the visible range (e.g., $1.2 \mu\text{m}$), then the optical thickness, the phase function (and also g) are approximately equal to those parameters for a nonabsorbing case [Kokhanovsky, 2004a]. It means that (assuming that the ground albedo is known or can be neglected as for cloudy scenes over ocean in the near infrared spectral region) the value of R given by equation (15) depends on just one free parameter, the single scattering albedo ω_0 . Therefore equation (15) can be considered as a single transcendent equation to find the single scattering albedo ω_0 (e.g., at $g = 0.74$ and τ given by equation (8)). After finding ω_0 , one can also determine the effective crystal radius $a_{ef} = 3v/s$. Here v is the average volume of crystals and s is the average surface area of crystals in the elementary volume of a cloud. One can also introduce the effective diameter $D_{ef} = 2a_{ef}$.

[10] Clearly the probability of photon absorption $\beta = 1 - \omega_0$ increases with the size of particles. The rate of this increase depends on the assumption of the particular shape. To avoid this shape dependence, we propose to retrieve not the effective size of particles itself but the particle absorption length (PAL) ℓ defined in such a way that

$$\beta(\ell) = (1 - \exp(-\ell/\ell_0))\beta_\infty, \quad (16)$$

where $\ell_0 = \lambda/4\pi\chi$ is the so-called penetration depth governed by the imaginary refractive index of crystals χ and $\beta_\infty \equiv \beta(\infty)$. Note that the value of β_∞ for convex particles in random orientation coincides with those of spheres independently on their shape [Kokhanovsky, 2004a]. This allows us to derive β_∞ using Mie theory. In particular, we find $\beta_\infty = 0.47$ for the real part of the ice refractive index $n = 1.3$. The law given by equation (16) is characteristic for many types of particles in the geometrical optics scattering domain as found by Kokhanovsky and Macke [1997]. Therefore equation (15) with account for equation (16) can be used for the determination of the PAL ℓ .

[11] The dependence of β on the attenuation parameter $c = D_{ef}/\ell_0$ calculated for spherical particles, hexagonal cylinders, and fractal particles is shown in Figure 1. Details for the calculations are specified in Table 1. We find that all these diverse forms follow the common law expressed by equation (16) very closely and

$$\ell = BD_{ef}, \quad (17)$$

where B depends on the habit of crystals. We find from data given in Figure 1: $B = 0.9$ for spheres, $B = 1.2$ for hexagonal prisms with parameters considered in Figure 1, and $B = 1.8$ for fractal particles at $n = 1.3$. We found that the accuracy of equation (16) increases for smaller β . Then errors of equation (15) are also smallest.

[12] That means that independently on the shape assumption we can derive the spatial distribution of the particle

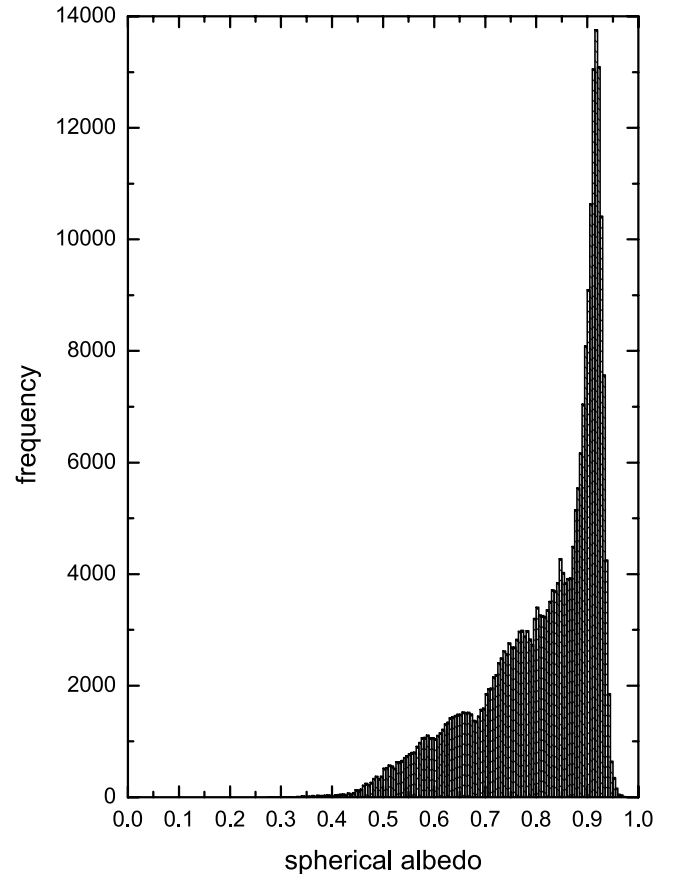


Figure 9. Spherical albedo frequency distribution.

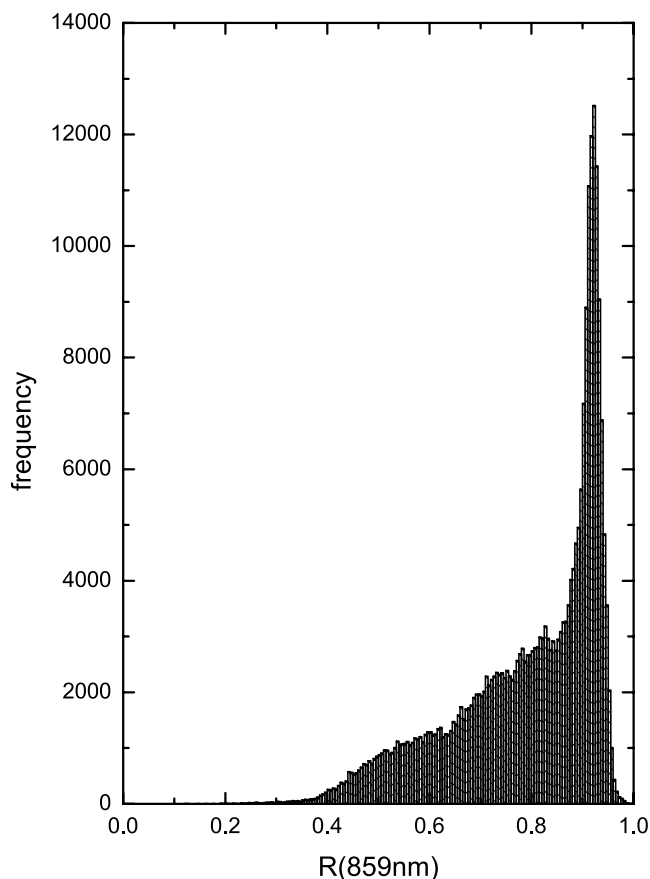


Figure 10. Frequency distribution of the top of atmosphere reflectance R at $\lambda = 859$ nm.

absorption lengths ℓ for crystalline clouds with complex and a priori unknown shapes of particles. This is a major result of this work.

[13] A priori assumptions on the shape of particles can bias the value $D_{ef} = \ell/B$ considerably. However, this is not the case for ℓ (see Figure 1). In many cases the value of D_{ef} itself is not needed (e.g., in climate research). Then the single scattering albedo is of particular importance and can easily be found from equation (16) using the retrieved value of ℓ (e.g., from satellite data) at a single wavelength (at least in the spectral region, where the real part of refractive index of ice n does not differ substantially from the value of n at the wavelength used in the retrieval of ℓ). This is the case for ice in the broad spectral region (e.g., 460–1700 nm, where $n \in [1.29, 1.31]$ [Kokhanovsky, 2004a]).

[14] The value of ℓ is only weakly influenced by the imaginary part of the refractive index as it follows from Figure 1. However, the particle absorption length is generally influenced by the refraction processes on the surface of a scatterer. In particular, we have for spheres as $n \rightarrow 1$: $B = 2/3 \approx 0.67$ [Kokhanovsky, 2004a] as compared to $B = 0.9$ at $n = 1.3$. The function $B(n)$ can be easily established for any particular shape or for a combination of shapes using geometrical optics calculations.

[15] However, the information on the shape distribution is not available, for example, in the operational ice cloud retrievals [Platnick *et al.*, 2003]. Therefore we believe that

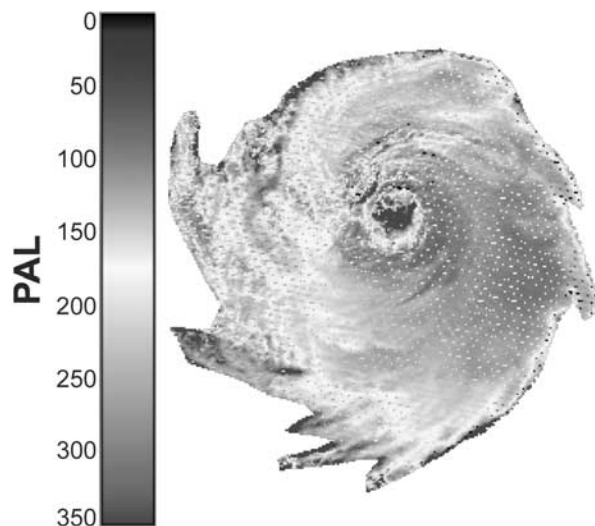


Figure 11. Retrieved particle absorption length map. See color version of this figure at back of this issue.

shape independent retrievals of ℓ as proposed in this paper are of a certain advantage.

3. Application of SACURA to MODIS Data

[16] The semianalytical ice cloud retrieval algorithm introduced above has been applied to data from the Mod-

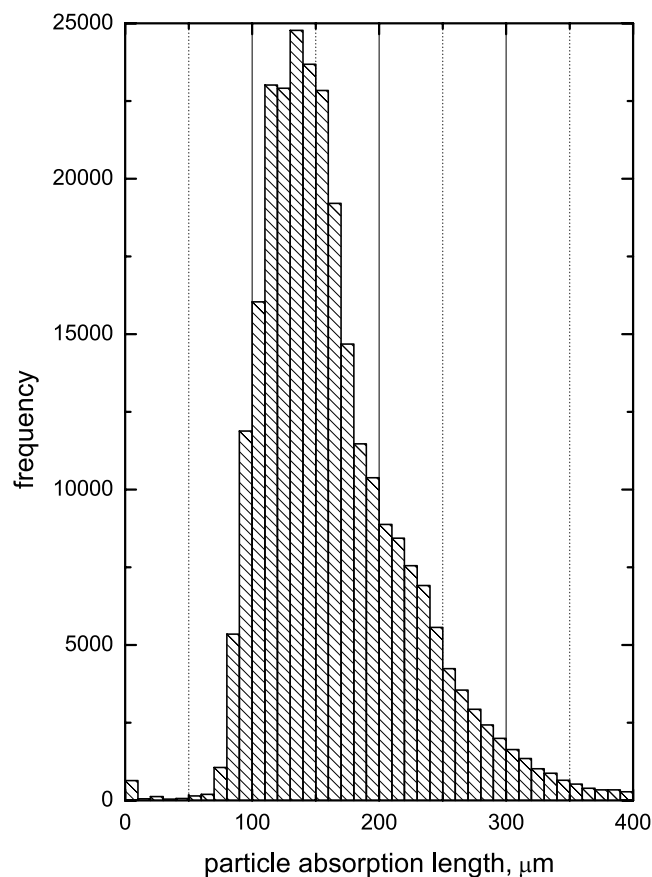


Figure 12. Statistical distribution of retrieved values of the particle absorption length.

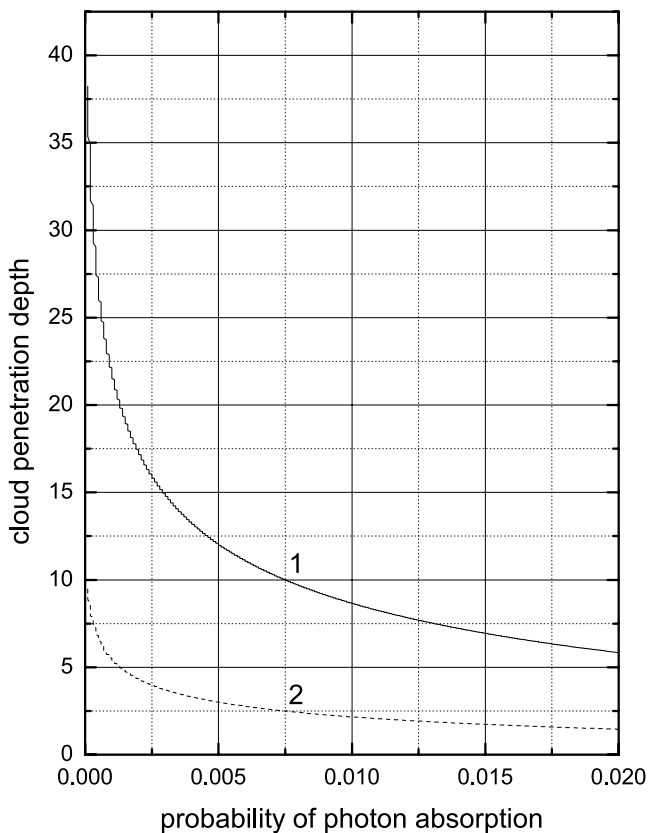


Figure 13. Dependence of the cloud optical penetration depth (line 1) and the cloud optical reduced penetration depth (line 2) on the probability of photon absorption [Kokhanovsky, 2004b].

erate Resolution Imaging Spectroradiometer (MODIS) [King *et al.*, 1992] aboard of the polar orbiting Terra/Aqua satellites which are part of the NASA Earth Observing System (EOS). MODIS has 36 channels between 0.4 and 14 μm and a spatial resolution between 250 and 1000 m. For the present study, a MODIS scene from 25 September 2005, 1615 UTC was used, showing Hurricane Jeanne just before its landfall southeast of Stuart (Florida) as a category 3 hurricane (see Figure 2). The data were supplied by NASA via the Distributed Active Archive Center (DAAC, <http://daac.gsfc.nasa.gov/>) and processed within an operational processing scheme [Nauss and Bendix, 2005]. The SACURA ice retrieval algorithm has been applied to the ice cloud regions around the eye of the hurricane which have been identified using NASA's thermodynamic cloud phase product which is based on the brightness temperature difference between the 8.5 μm and 11 μm MODIS channels [Platnick *et al.*, 2003].

3.1. Reduced Optical Thickness

[17] The 859 and 1240 nm MODIS channels have been selected for the cloud property retrieval over the ice cloud fields associated with Hurricane Jeanne (see Figure 2). It should be pointed out that usually the 1640 nm channel is used in cloud effective size retrieval procedures [Platnick *et al.*, 2003]. However, ice is approximately 20 times less absorptive at 1240 nm than at 1640 nm, which enables the

sensing of larger vertical cloud columns. In addition the assumption $\omega_0 \rightarrow 1$ is not violated for most of the pixels. Therefore the simple formulation based on equation (15) can be used (note that both channels are almost free of gaseous absorption) as it can be seen from Figure 3. In contrast to ice clouds, the 1640 nm channel should preferably be used for the retrieval of droplet sizes in water clouds. This is due to the low absorption of light by water droplets at 1240 nm and therefore missing information on the droplet size within this channel signal (see Figure 3). The situation is very different for crystalline media as in the case for the hurricane event studied in the present paper.

[18] The dependence of the measured reflection function at 1240 nm to that at 859 nm is presented in Figure 4 for the central core of the hurricane. It follows that both reflectances almost coincide at $R(859 \text{ nm}) < 0.3$. Then, of course, the retrieval of the ice crystal size using these channels is not possible. For thicker clouds, values of $R(1240 \text{ nm})$ are lower than those at 859 nm because of the increased importance of light absorption effects for larger wavelengths by large ice crystals. In particular, light absorption at 859 nm by ice is two orders of magnitude lower than that at 1240 nm. So the level of deviations of points from a straight line in Figure 4 can be used to estimate the size of crystals as discussed in the previous section. The optical thickness is determined from measurements at 859 nm using equation (5). We suppose that the value of τ derived at 859 nm coincides with that at 1240 nm. This is an accurate assumption due to the spectral neutrality of the ice cloud extinction coefficient in the near IR.

[19] A statistically insignificant number of points deviate from the general rule $R(859) > R(1240 \text{ nm})$ (see Figure 4). These points are not consistent with the model of a thick plane-parallel cloud over a black surface under the assumption of very low levels of gaseous absorption used in this paper. So we conclude that either our model is not valid for these selected pixels of a hurricane or there are problems with the measurements. Most likely, the deviation is caused by 3-D radiation effects especially in the eye wall region that are not accounted for in our retrieval model. The derived map of the ROT is given in Figure 5. We see that values of δ are larger than 15 in the vicinity of the core. They are smaller than 10 on the periphery. The correspondent frequency histogram is shown in Figure 6. It follows that the frequency distribution $f(\delta)$ has two maxima, reflecting different conditions in the central parts of the hurricane with the modal value of $\delta \approx 14$ as compared to the periphery where the modal value of δ is close to 3. Retrievals for $\delta < 1$ are less accurate because of the poor accuracy of approximation (4) for thin clouds.

[20] The correlation plot for the retrieved reduced optical thickness against the MOD06 algorithm derived cloud optical thickness τ_m is presented in Figure 7. One must expect that $\delta = (1 - g)\tau_m$. This is indeed the case as one finds $\tau_m \approx 5\delta$ from data given in Figure 7, which corresponds to $g \approx 0.8$.

[21] We do not show the SACURA-derived spatial distribution of the optical thickness τ because it is influenced by the vertical distribution of the parameter $\varepsilon = 1 - g$, which presumably changes from 0.25 for ice clouds in the upper part of the hurricane to 0.15 for water clouds

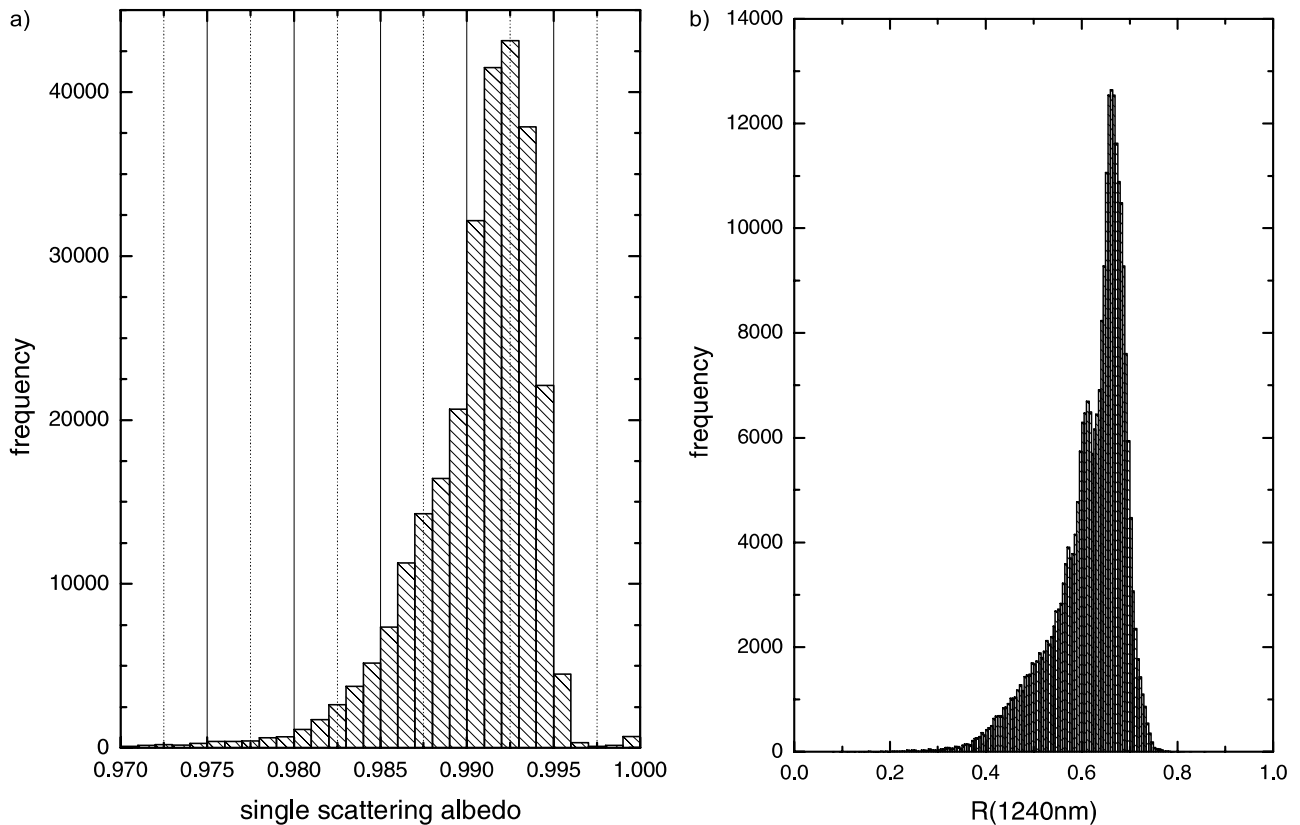


Figure 14. Statistical distribution of retrieved values of (a) the single scattering albedo and (b) the frequency distribution of the top of atmosphere reflectance R at $\lambda = 1240$ nm.

underneath. Depending on assumptions of the vertical profile $g(z)$, where z is the vertical coordinate, considerably different values of τ can be derived.

[22] The correlation of δ with the MODIS-derived cloud temperature T is shown in Figure 8. Even there is no such clear correlation as in Figure 7, a tendency exists for thicker clouds to have smaller cloud top temperatures. This can be easily understood because of the fact that such clouds are also geometrically thicker and therefore they penetrate to higher altitudes, where T is rather small. The minimal values of T are close to -80°C in the case studied. It follows that $T < -20^\circ\text{C}$ for most of retrievals confirming that we really consider ice and not water clouds in this study.

[23] Equation (6) allows us to find the spherical albedo of a hurricane $r_0 = 1 - t_0$ at the wavelength 859 nm. This is shown in Figure 9. It follows that the modal value of r_0 is close to 0.91 for the hurricane core. The frequency distribution $f(r_0)$ increases rather slowly with r_0 and then abruptly drops out at $r_0 \approx 0.92$. This means that the frequency distribution presented in Figure 9 follows a beta distribution law common for bounded processes (e.g., the maximal value of r_0 is 1 by definition). Similar trend is seen in the reflection function distribution presented in Figure 10.

3.2. Particle Absorption Length

[24] We do not present the effective crystal size in this section, which is a common practice for modern cloud remote sensing techniques [Platnick *et al.*, 2003], but rather the particle absorption length, which is much more robust against assumptions of crystals habits. To find the PAL, we need to

know not only δ but also τ (see equations (11) and (14)). The transfer from δ to τ makes no problem for pure crystalline clouds ($\varepsilon \approx 0.25$) but in the case considered here we face a multilayered cloud system with both ice crystals and water droplets. So the retrieval generally becomes much more complicated and, as it was specified above, the profile $\varepsilon(z)$ is not known a priori. To avoid this problem, we assumed in equation (11): $\varepsilon = 1 - g \approx 0.25$. This may bias results for thin clouds but actually has no effect on most of our retrievals because for the hurricane case the cloud thickness is quite large and the asymptotic limit of a semi-infinite cloud is almost reached at the 1240 nm. Therefore the value of τ is not a crucial parameter of the retrieval in this specific case. This also means that the two last terms in equation (11) make only a small contribution for optically thick clouds with large crystals. Interestingly, equation (15) can be solved analytically with respect to y (and therefore β , ℓ) as $\tau \rightarrow \infty$. Then the last term in equation (15) can be dropped.

[25] The map of the particle absorption length derived from our bispectral algorithm as underlined above is shown in Figure 11. We see that in most of the cases the PAL is in the region 100–150 μm . The spatial distribution of ℓ does not have the symmetry with respect to the core. In particular, larger values of ℓ and maybe also larger hurricane momentum and larger mass, are observed in the western part, where the direction of the hurricane propagation is located. It could be of a practical value to confirm larger values of the PAL in the hurricane propagation direction when studying more hurricane

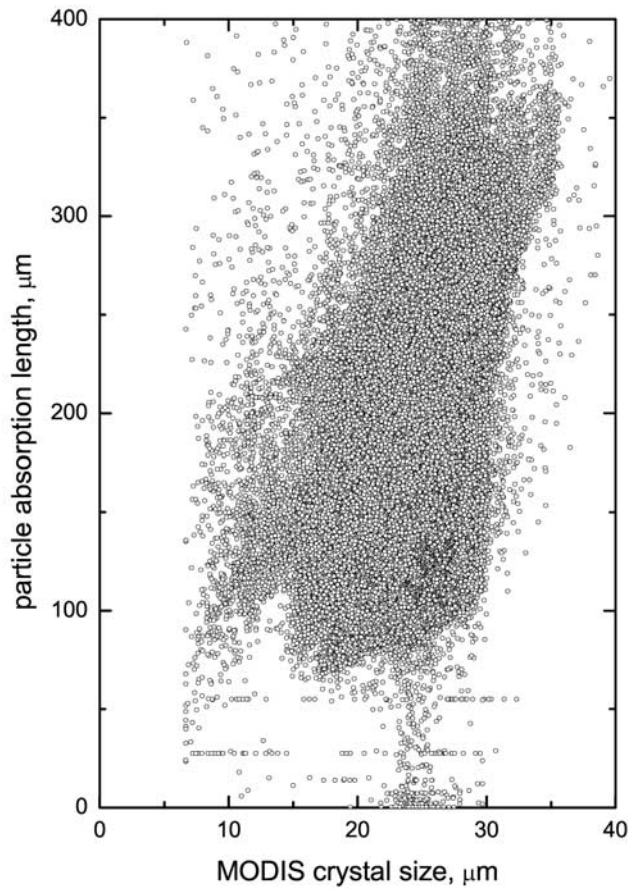


Figure 15. Correlation between the particle absorption length and the effective radius a_{ef} . The values of a_{ef} are derived using the MODIS cloud retrieval algorithm.

events. Note that clouds inside the eye are thin and therefore retrievals of both ℓ and δ using SACURA are not reliable. Then the standard lookup table approach must be applied.

[26] The correspondent frequency histogram is shown in Figure 12. It follows that the frequency distribution $f(\ell)$ has the maximum at $\ell \approx 0.14$ mm and the distribution $f(\delta)$ has just one mode as compared to $f(\ell)$ (see Figure 6). This confirms a more uniform distribution of crystal sizes in the hurricane as compared to the total water distribution. It should be remembered that the wavelength 1240 nm used for the particle sizing has a finite penetration depth. So our estimations are limited to depths $L < L_p$, where L_p is the geometrical penetration depth defined as $L_p = \tau_p / \sigma_{ext}$, where σ_{ext} is the cloud extinction coefficient and τ_p is the optical penetration depth defined by Kokhanovsky [2004b] as the value of optical thickness such that $R(\tau_p) = 0.9R(\infty)$, where $R(\infty)$ is the reflection function for a semi-infinite layer. Clearly, τ_p depends on ω_0 . In particular, we present the dependence of τ_p (and also the reduced penetration optical thickness $\delta_p = (1 - g)\tau_p$ in Figure 13 for nadir observation and the solar zenith angle of 60° . It was assumed that $g = 0.75$ and the phase function has been approximated by that for fractal particles [Macke *et al.*, 1996]. The frequency distribution of ω_0 derived using SACURA is shown in Figure 14a. The distribution of the single scattering albedo has a similar shape as the frequency distribution of the reflection function $R(1240 \text{ nm})$ shown in Figure 14b.

[27] It follows from Figure 14a that the modal value of the single scattering albedo is equal to 0.9925. This confirms the applicability of the weak absorption approximation to the case studied and also allows the estimation of τ_p using equation (8) given by Kokhanovsky [2004b]. One obtains from Figures 13 and 14a that the modal value of β equals 0.0075, the modal value of τ_p is approximately equal

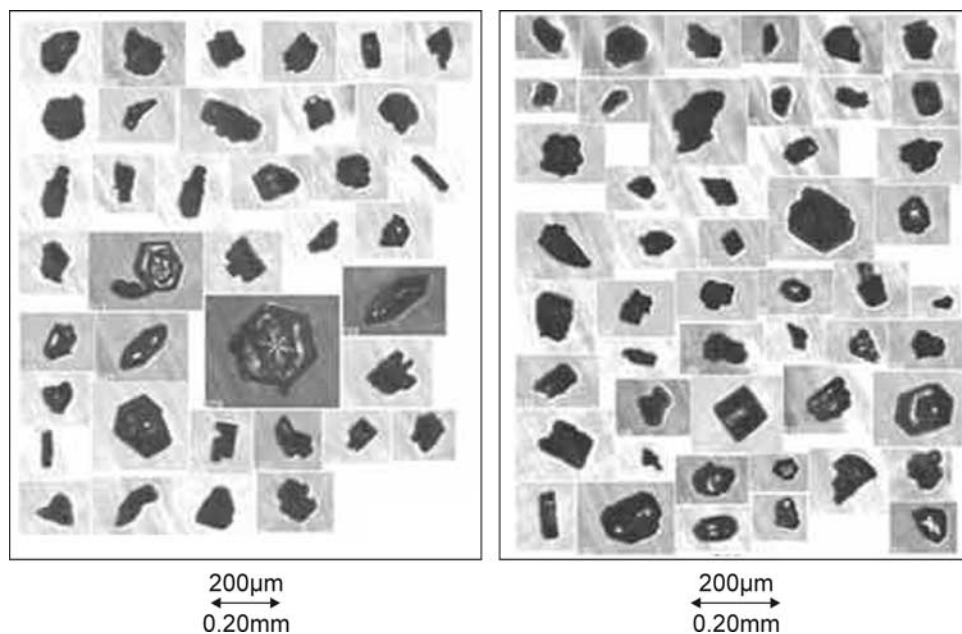


Figure 16. Images of ice crystals in hurricane Humberto, 2001 (A. Heymsfield, private communication, 2004).

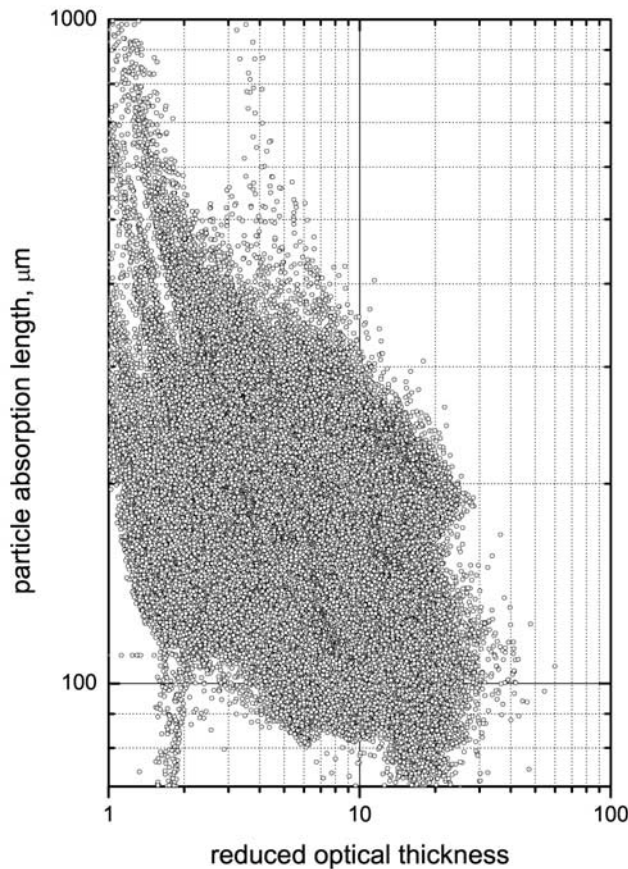


Figure 17. Correlation between the particle absorption length and the reduced optical thickness as derived by SACURA.

to 10, and the modal value of δ_p approximately equals 2.5 at $\lambda = 1240$ nm.

[28] Taking into account that the modal value of δ at $\lambda = 859$ nm equals 14 for the hurricane core, we obtain that the wavelength 1240 nm senses approximately 20% of the hurricane vertical extent starting from its top ($\delta_p \approx 2.5$). It means that remote sensing of crystals at the wavelength 1240 nm allows us to perform an averaging for quite large vertical columns.

[29] Because of the general increase in the size of the ice crystals with the distance from the cloud top height downward, one may expect that sizes derived for less penetrated wavelengths are generally smaller. In particular, we show the correlation plot between the effective crystal radius as derived by the MOD06 product at 1640 nm versus the SACURA-derived PAL at $\lambda = 1240$ nm in Figure 15. We see a clear correlation between these two parameters with values of $\ell \approx 10a_{ef}$.

[30] Unfortunately, we are not aware of any aircraft campaigns to collect particles in the hurricane studied here. However, such results are available for Hurricane Humberto (see Figure 16). The average maximum dimension of crystals collected at the top of Humberto (≈ 0.15 mm) is close to that given in Figure 12. So we may assume that the PAL may well correlate with the maximal crystal dimensions D_{\max} measured in the field campaigns. This assumption must be checked in future research.

[31] In conclusion, we present correlation plots of the derived values of ℓ with δ and T (see Figures 17 and 18). It follows that the particle absorption length decreases with the reduced optical thickness and the value of ℓ increases with temperature. Both facts indicate that crystals at higher atmosphere levels have smaller sizes. In particular, it follows from Figure 18 that

$$\ell = ae^{bT}, \quad (18)$$

where $a = 550 \mu\text{m}$, $b = 0.02$ and T is given in $^{\circ}\text{C}$. A similar expression (but for D_{\max}) has been found by *Ivanova et al.* [2004] using a limited number of in situ measurements. They reported the following values of parameters: $a = 332.58 \mu\text{m}$ and $b = 0.0335$. An interesting consequence of equation (18) is the possibility to estimate (in the statistical sense) the cloud temperature from the measurements of the particle absorption length.

4. Conclusions

[32] The semianalytical algorithm proposed by *Kokhanovsky et al.* [2003] has been extended to the case of ice clouds. Our retrieval technique is applicable only to the case of optically thick extended cloudiness as selected for this study on the basis of MODIS measurements. The paper gives

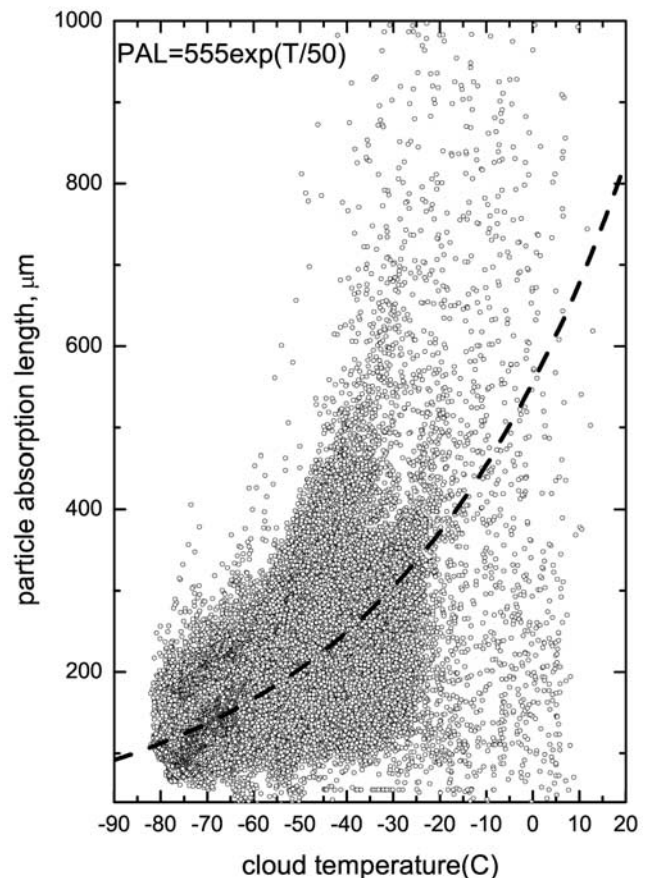


Figure 18. Correlation between the particle absorption length and the cloud temperature. The cloud temperature was derived using the MODIS cloud retrieval algorithm.

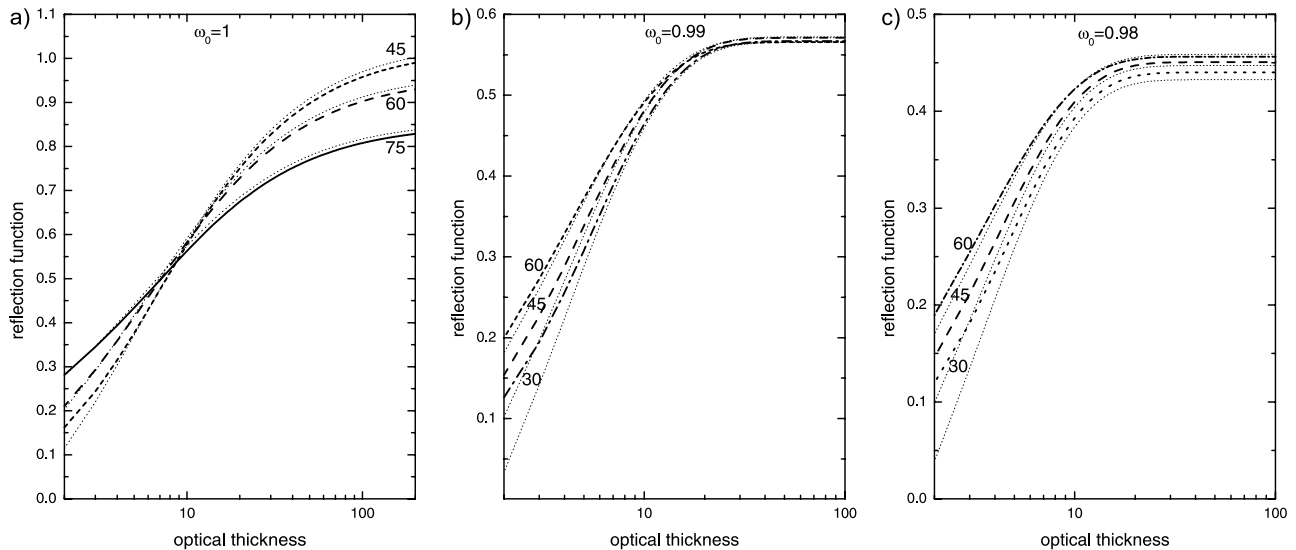


Figure A1. Dependence of reflection function on the optical thickness calculated using the exact radiative transfer code for the black underlying surface, nadir observation, different solar angles (30°, 45°, 60°, and 75°) and (a) $\omega_0 = 1$, (b) $\omega_0 = 0.99$, and (c) $\omega_0 = 0.98$ for the phase function of fractal ice crystals as described by *Mishchenko et al.* [1999]. Dotted lines give results as obtained from the analytical equation (15) with account for equations (12)–(14). The value of g is equal to 0.7524 [*Mishchenko et al.*, 1999] for the phase function under study.

the first application of SACURA to ice cloud fields. The results obtained allow us to study the complex structure of the hurricane with a spatial resolution of 1 km not accessible to microwave techniques usually used to monitor hurricanes (see Figures 5 and 11).

[33] We proposed two new parameters to be remotely sensed from satellites over thick ice clouds: the particle absorption length and the reduced optical thickness. These parameters are less biased as compared to a_{ef} and τ and therefore allow us to avoid the great uncertainty associated with the retrieval of crystal sizes from airborne and spaceborne optical instruments. We underline that the retrieved values of a_{ef} and τ strongly depend on a priori assumptions with respect to the habits of crystals.

[34] First maps of the spatial distribution of the reduced optical thickness and the particle absorption lengths are derived using MODIS bispectral measurements at 859 nm and 1240 nm free of gaseous absorption. For the case studied, the reduced optical thickness has two modes ($\delta \approx 3$, $\delta \approx 14$) and the most frequent value of the particle absorption length is 0.14 mm.

[35] The information on typical sizes of ice crystals in hurricanes is of importance in understanding the hurricane dynamics and also for weather prediction, radiative transfer models, convective dehydration, and stratospheric chemistry [*Webster and Heymsfield*, 2003]. Large values of ℓ obtained in our work suggest large near-surface condensate transported to upper levels by deep convection. Normally, crystal sizes are much smaller for ice clouds originated close to the tropopause [*Garrett et al.*, 2004] because of many factors including first of all the shortage of water vapor at high altitudes.

[36] The retrieved values of ℓ for thinner clouds may be biased because of the possible broken clouds conditions. At this stage it is difficult to relate the value of ℓ to the

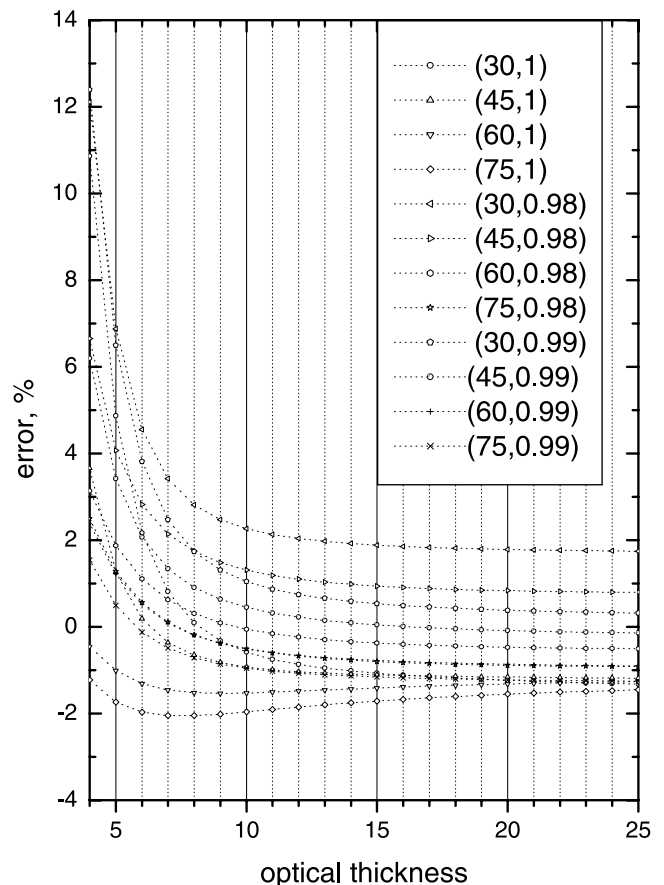


Figure A2. Errors of equation (15) calculated under the same conditions as in Figure A1. The first number in parentheses gives the observation angle in degrees, and the second number is the single scattering albedo.

geometrical characteristics of particles. However, we may assume that $\ell \approx D_{\max}$, where D_{\max} is the maximum dimension of the particle. This is approximately the case for ice spheres, where $\ell \approx 0.9D_{\max}$ (see Figure 1). Here D_{\max} is equal to the average diameter for spheres.

[37] The retrieved values of ℓ must be in the range of experimentally measured values of D_{\max} derived from in situ experiments. We found that the most frequently occurring values of ℓ derived using SACURA well correspond to in situ measurements of the maximal size of crystals in a hurricane (see Figure 16 and also <http://earthobservatory.nasa.gov/Newsroom/NasaNews/2002/200204299301.html>). Clearly, this assumption should be validated in future. The modal values of D_{\max} are usually in the range 50–300 μm as was found by in situ measurements [Baum *et al.*, 2005a]. The majority of the retrieved particle absorption lengths ℓ also belongs to this interval (see Figure 12).

Appendix A: Accuracy of Approximate Equation for the Reflection Function

[38] The accuracy of main equation (15) is studied in Figures A1 and A2 for a specific case of the black underlying surface, nadir observation and wavelengths 859 and 1240 nm for the several values of ω_0 and selected solar zenith angles. The fractal model of scatterers as discussed by Macke *et al.* [1996] and Mishchenko *et al.* [1999] has been used to calculate the phase function. We find that the error increases for smaller values of the single scattering albedo and the optical thickness, being smaller than 5% at $\tau \geq 6$ and $\omega_0 \geq 0.98$. The values of τ and also ω_0 at 1240 nm were larger than values reported above for a great majority of cases studied in this work. Therefore we estimate that the error of equation (15) was below 2% for most of retrievals performed. Even smaller errors (typically, below 1%) occur for the parameter β calculated using equation (16) as compared to the ray tracing code at $\omega_0 \geq 0.98$. The parameter g does not change considerably in the spectral range from 859 to 1240 nm for fractal particles and close to the assumed value of 0.74 (within 1%). Therefore we conclude that our errors are generally below or close to calibration errors of MODIS.

[39] The error propagation analysis for SACURA has been performed by Kokhanovsky *et al.* [2003]. Therefore we do not repeat this analysis here and refer to our previous work.

[40] **Acknowledgments.** This work was supported by DFG project BU 688/8-1, by the German Federal Ministry for Education and Research (BMBF) in the scope of the GLOWA-Danube project 07 GWK 04 "Rainfall Retrieval," and the Erich-Becker Foundation of the Frankfurt Airport AG (Germany). The authors are grateful to the NASA DAAC MODIS team for providing experimental data and to J. P. Burrows, A. Macke, S. Platnick, V. V. Rozanov, and E. P. Zege for important discussions on the subject of this paper. We are thankful to A. Heymsfield for providing Figure 16 and B. A. Baum for providing his unpublished papers to us.

References

- Baum, B. A., P. Yang, A. J. Heymsfield, and S. M. Thomas (2005a), Bulk scattering properties for the remote sensing of ice clouds. 1: Microphysical data and models, *J. Appl. Meteorol.*, in press.
- Baum, B. A., P. Yang, A. J. Heymsfield, and S. M. Thomas (2005b), Bulk scattering properties for the remote sensing of ice clouds. 2: Narrowband models, *J. Appl. Meteorol.*, in press.
- Garrett, T. J., P. V. Hobbs, and H. Gerber (2001), Shortwave, single-scattering properties of Arctic ice clouds, *J. Geophys. Res.*, 106(D14), 15,155–15,172.
- Garrett, T. J., A. J. Heymsfield, M. J. McGill, B. A. Ridley, D. G. Baumgardner, T. P. Bui, and C. R. Webster (2004), Convective generation of cirrus near the tropopause, *J. Geophys. Res.*, 109, D21203, doi:10.1029/2004JD004952.
- Gerber, H., Y. Takano, T. J. Garrett, and P. V. Hobbs (2000), Nephelometer measurements of the asymmetry parameter, volume extinction coefficient, and backscatter ratio in Arctic clouds, *J. Atmos. Sci.*, 57, 3021–3034.
- Ivanova, D. C., D. L. Mitchell, and G. M. McFarquhar (2004), A trimodal size distribution parameterization for tropical cirrus clouds, paper presented at 14th ARM Science Team Meeting, Atmos. Radiat. Meas., Albuquerque, N. M., 22–26 March.
- King, M. D. (1987), Determination of the scaled optical thickness of clouds from reflected solar radiation measurements, *J. Atmos. Sci.*, 44, 1734–1751.
- King, M. D., Y. J. Kaufman, W. P. Menzel, and D. Tanre (1992), Remote sensing of cloud, aerosol, and water vapor properties from the moderate resolution imaging spectrometer (MODIS), *IEEE Trans. Geosci. Remote Sens.*, 30, 2–27.
- Kokhanovsky, A. A. (2003), Optical properties of irregularly shaped particles, *J. Phys. D Appl. Phys.*, 36, 915–923.
- Kokhanovsky, A. A. (2004a), *Light Scattering Media Optics: Problems and Solutions*, Springer, New York.
- Kokhanovsky, A. A. (2004b), The depth of sunlight penetration in cloud fields for remote sensing, *IEEE Trans. Geosci. Remote Sens. Lett.*, 1, 242–245.
- Kokhanovsky, A. A. (2005), Reflection of light from particulate media with irregularly shaped particles, *J. Quant. Spectrosc. Radiat. Transfer*, 96, 1–10.
- Kokhanovsky, A. A., and A. Macke (1997), Light scattering and absorption characteristics of large nonspherical particles, *Appl. Opt.*, 36, 8785–8790.
- Kokhanovsky, A. A., and V. V. Rozanov (2004), The physical parameterization of the top of atmosphere reflection function for a cloudy atmosphere-underlying surface system: The oxygen A-band study, *J. Quant. Spectrosc. Radiat. Transfer*, 85, 35–55.
- Kokhanovsky, A. A., and W. von Hoyningen-Huene (2004), Optical properties of a hurricane, *Atmos. Res.*, 69, 165–183.
- Kokhanovsky, A. A., V. V. Rozanov, E. P. Zege, H. Bovensmann, and J. P. Burrows (2003), A semianalytical cloud retrieval algorithm using backscattered radiation in 0.4–2.4 μm spectral region, *J. Geophys. Res.*, 108(D1), 4008, doi:10.1029/2001JD001543.
- Macke, A., J. Mueller, and E. Raschke (1996), Scattering properties of atmospheric ice crystals, *J. Atmos. Sci.*, 53, 2813–2825.
- Mishchenko, M. I., J. M. Dlugach, E. G. Yanovitskij, and N. T. Zakharova (1999), Bidirectional reflectance of flat, optically thick particulate layers: An efficient radiative transfer solution and applications to snow and soil surfaces, *J. Quant. Spectrosc. Radiat. Transfer*, 63, 409–432.
- Nakajima, T., and M. D. King (1992), Asymptotic theory for optically thick layers: Application to the discrete ordinates method, *Appl. Opt.*, 31, 7669–7683.
- Nauss, T., and J. Bendix (2005), An operational MODIS processing scheme for PC dedicated to direct broadcasting applications in meteorology and Earth sciences, *Comput. Geosci.*, 31(6), 804–808.
- Nauss, T., A. A. Kokhanovsky, T. Y. Nakajima, C. Reudenbach, and J. Bendix (2005), The intercomparison of selected cloud retrieval algorithms, *Atmos. Res.*, in press.
- Platnick, S., M. D. King, S. A. Ackerman, W. P. Menzel, B. A. Baum, J. C. Riedi, and R. A. Frey (2003), The MODIS cloud products: Algorithms and examples from Terra, *IEEE Trans. Geosci. Remote Sens.*, 41, 459–473.
- Rozanov, A. V., V. Rozanov, M. Buchwitz, A. Kokhanovsky, and J. P. Burrows (2005), SCIATRAN 2.0: A new radiative transfer model for geophysical applications in the 175–2400 nm spectral region, *Adv. Space Res.*, in press.
- Sassen, K., and K. N. Liou (1979), Scattering of polarized laser light by water droplets, mixed-phase and ice crystal clouds, part I: Angular scattering patterns, *J. Atmos. Sci.*, 36, 838–851.
- van de Hulst, H. C. (1980), *Multiple Light Scattering: Tables, Formulas and Applications*, Elsevier, New York.
- Webster, C. R., and A. Heymsfield (2003), Water isotope ratios D/H, $^{18}\text{O}/^{16}\text{O}$, $^{17}\text{O}/^{16}\text{O}$ in and out of clouds map dehydration pathways, *Science*, 302, 1742–1745.

A. A. Kokhanovsky, Institute of Remote Sensing, University of Bremen, O. Hahn Allee 1, D-28334 Bremen, Germany. (alexk@iup.physik.uni-bremen.de)

T. Nauss, Laboratory of Climatology and Remote Sensing, Marburg University, Deutschhausstr. 10, D-35032 Marburg, Germany.

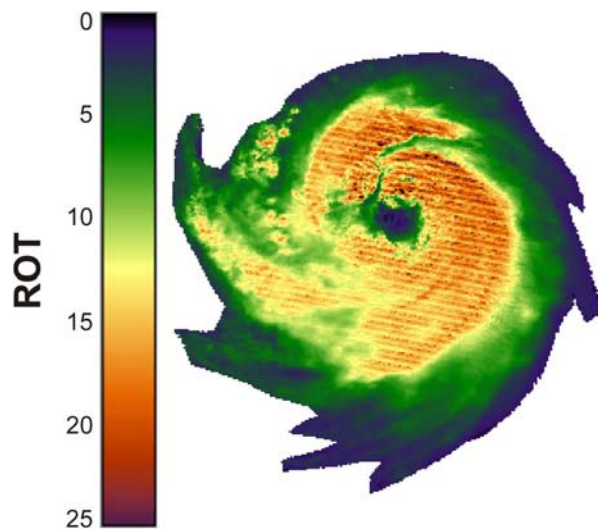


Figure 5. Reduced optical thickness map.

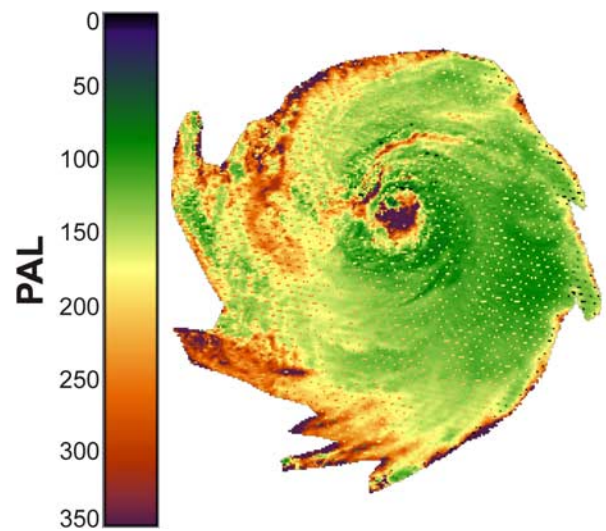


Figure 11. Retrieved particle absorption length map.